ACS Biomaterials SCIENCE & ENGINEERING

pubs.acs.org/journal/abseba

Article

Full Remission of CAR-Deficient Tumors by DOTAP-Folate Liposome Encapsulation of Adenovirus

Ching-Hsin Huang, Tao Dong, Abraham T. Phung, Jaimin R. Shah, Christopher Larson, Ana B. Sanchez, Sarah L. Blair, Bryan Oronsky, William C. Trogler, Tony Reid, and Andrew C. Kummel*

Cite This: *ACS Biomater. Sci. Eng.* 2022, 8, 5199–5209

Read Online

ACCESS | Metrics & More | Article Recommendations | Supporting Information

ABSTRACT: Adenovirus (Ad)-based vectors have shown considerable promise for gene therapy. However, Ad requires the coxsackievirus and adenovirus receptor (CAR) to enter cells efficiently and low CAR expression is found in many human cancers, which hinder adenoviral gene therapies. Here, cationic 1,2-dioleoyl-3-trimethylammonium-propane (DOTAP)-folate liposomes (Df) encapsulating replication-deficient Ad were synthesized, which showed improved transfection efficiency in various CAR-deficient cell lines, including epithelial and hematopoietic cell types. When encapsulating replication-competent oncolytic Ad (TAV255) in DOTAP-folate liposome (TAV255-Df), the adenoviral structural protein, hexon, was readily produced in CAR-deficient cells, and the tumor cell killing ability was 5× higher than that of the non-encapsulated Ad. In CAR-deficient CT26 colon carcinoma murine models, replication-competent TAV255-Df treatment of subcutaneous tumors by intratumoral injection resulted in 67% full tumor remission, prolonged survival, and anti-cancer immunity when mice were rechallenged with cancer cells with no further treatment. The preclinical data shows that DOTAP-folate liposomes could significantly enhance the transfection efficiency of Ad in CAR-deficient cells and, therefore, could be a feasible strategy for applications in cancer treatment.

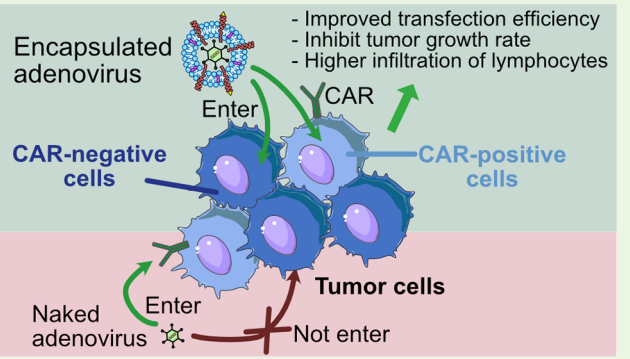

KEYWORDS: *oncolytic virus, liposome, folate targeting, coxsackievirus and adenovirus receptor, DOTAP*

1. INTRODUCTION

Immunotherapy is emerging as an essential part of cancer treatment with fewer side effects and better efficacy than the traditional cytotoxic chemotherapy. One example is virotherapy, which is a versatile therapeutic cancer treatment.[1−4] It can be used for direct oncolysis induced by the viral replication,[5,6] as well as a cancer vaccine to activate an immune response against cancers.[7−9] Among viruses, adenovirus (Ad) is a robust platform for gene therapy because the genome of Ad is well characterized and easy to manipulate.[10] Particularly for cancer gene therapy, recombinant Ad can carry various genes and transfect a wide range of cells at different stages. Ad is now being studied in many clinical trials approved by the FDA.[11,12] However, most Ad serotypes require cellular coxsackievirus and adenovirus receptors (CARs) to enter and transfect the cells efficiently. Ad utilizes CAR as its primary attachment receptor.[13] After binding to the CAR, it triggers clathrin-mediated endocytosis (Scheme 1).[14,15] Ad enters the endosomes and follows a series of uncoating processes. The escaped Ad docks to the nuclear membrane and imports its DNA into the nucleus for subsequent transcription and replication.[16,17] The CAR expression is extremely heterogenous in cancers,[18,19] limiting effectiveness in cells with low CAR expression.

To circumvent the need for CAR-dependent cell entry, several studies have used liposomes and nanoparticles to deliver Ad and improve transfection. Various 1,2-dioleoyl-3-trimethylammonium-propane (DOTAP) liposomes or commercial agents (Lipofectin) were used to encapsulate Ad to enhance the adenoviral gene delivery in CAR-deficient cells (Table 1). Lipofectin-encapsulated virus shows approximately 40% of the transfection rate in CAR-negative CT26 cells. Han et al. used DOTAP, 1,2-dioleoyl-3-phosphatidylethanolamine (DOPE), and 1,2-distearoyl-*sn*-glycero-3-phosphoethanolamine-*N*-[methoxy(poly-ethylene glycol)-2000] [PEG(2000)-PE] to encapsulate Ad and achieved only 66% transfection at multiplicity of infection (MOI) = 100 in CAR-negative cells; in order to achieve 97% of cells being transfected, 500 MOI of encapsulated Ad had to be used.[20] Kim et al. employed a DOTAP and 1,2-dimyristoyl-*sn*-glycero-3-phosphocholine

Received: August 15, 2022
Accepted: November 3, 2022
Published: November 17, 2022

Scheme 1. Naked Ad and Coated Ad Entering Cells[a]

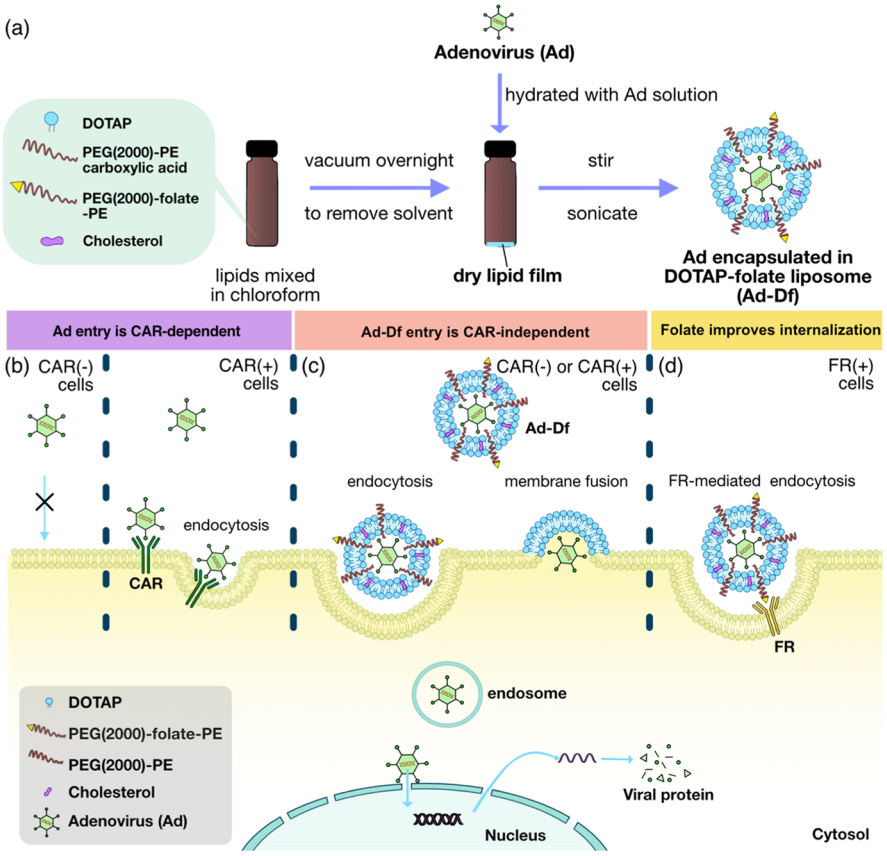

[a](a) Synthesis of Ad-encapsulated DOTAP-folate liposome (Ad-Df). (b) Ad uses the CAR to enter the cells. For cells expressing low to null CAR, Ad does not efficiently enter and transfect cells. Tumors have various levels of CAR expression, and many tumor cells are resistant to Ad-based gene transfer because of low CAR expression. (c) Ad-Df can enter cells through endocytosis or membrane fusion when the target cells do not express CAR.[32−34] Therefore, Ad-Df is capable of transfecting both CAR-positive and CAR-negative cells. (d) Ad-Df also contains folate-conjugated lipid that enhances the cellular uptake into FR-positive cells by FR-mediated endocytosis. FR is commonly expressed or even overexpressed on tumor cells, including breast, lung, colorectal, and ovarian cancers.[16,37,38] After internalization of Ad-Df in cells, it is likely that the Ad is released due to liposome membrane destabilization from the interaction between the liposomal lipid and cytoplasmic lipid.[39,40]

Table 1. Comparison of Transfection Percentage in CAR-Deficient Cells Using Ad Encapsulated in DOTAP Liposomes or Commercial Agents[a]

formula (molar ratio)	cell line (car-negative)	MOI	transfection %	refs
DOTAP/Chol/PEG-Folate-PE/PEG-PE (1:0.26:0.01:0.02)	CT26	200	91	current study
Lipofectin (DOTMA/DOPE) (1:1.11)	CT26	500	40	commercial liposomes[20]
Lipofectin (DOTMA/DOPE) (1:1.11)	CT26	100	15	commercial liposomes[20]
DOTAP/DMPC/Chol/PEG-PE (6:0:6:0.06)	B16−F10	167	90	21
DOTAP/Chol (1:1)	B16−F10	100	65	29
DOTAP/Chol (1:1)	3T3	1000 vp/cell	80	30
DOTAP/Chol (1:1)	CHO	1000 vp/cell	60	30
DOTAP/DOPE/PEG-PE (1:1:0.01)	CT26	500	97	20
DOTAP/DOPE/PEG-PE (1:1:0.01)	CT26	100	66	20
DOTAP/DOPE/PEG-PE (1:1:0.01)	U87MG	500	85	22
DOTAP/DOTMA/CHOL (1:1:0.1)	CT26	n.i.	68	31

[a]n.i. means "not indicated". N/A means "not applicable" because the study used a non-viral vector to transfect cells.

(DMPC) liposome with a 1,2-distearoyl-*sn*-glycero-3-phosphoethanolamine-*N*-[methoxy(polyethylene glycol)-5000] [PEG(5000)-PE] modification to deliver Ad to CAR-negative B16F10 cells at MOI = 167 and found that about 90% of the cells were transfected.[21] Lee et al. encapsulated Ad in DOTAP−DOPE liposomes modified with PEG(2000)-PE to transfect CAR-negative U87MG, but 500 MOI was required to transfect ∼85% of the cells.[22] Oncolytic virus treatments were reported to induce adverse events such as fever, fatigue, chills, nausea, and vomiting.[4,23] Therefore, efficient transfection at low MOI is critical to improve the clinical safety and effectiveness.

Note that the present formation differs from the other reported DOTAP encapsulation formations due to (a) the incorporation of folate, (b) incorporation of both cholesterol (to

https://doi.org/10.1021/acsbiomaterials.2c00966
ACS Biomater. Sci. Eng. 2022, 8, 5199−5209

increase stability[24]) and PEG-PE (to reduce the serum protein opsonins[25]), and (c) preparation by sonication instead of extrusion. Other studies with in vivo testing, which showed full remission, employed extracellular vesicles-mimetic encapsulation of Ad.[26] However, the extracellular vesicles-mimetic encapsulation of adenoviruses requires more complicated preparation processes compared to liposomes. Bruckheimer et al.[27] and Liang et al.[28] used similar ingredients (DOTAP + folate + cholesterol) to prepare liposomes, but they delivered non-viral vectors which cannot replicate inside the infected cells to induce cell death.

In the present study, Ad was encapsulated in positively charged DOTAP-folate liposomes (Ad-Df in Scheme 1a) to facilitate viral attachment to the negatively charged cell membranes and, thus, to eliminate the need of the CAR for Ad cell entry (Scheme 1b). According to the literature, the cationic liposome and Ad assembly can enter cells through endocytosis and membrane fusion that facilitate the Ad internalization without a need for CAR, thereby enhancing the transfection (Scheme 1c).[32−34] However, more investigations will be needed to document the phenomena in breast cancer tissues for the present study. Folate-modified lipids in the liposome formula can further improve the cellular uptake of Ad-Df by attaching to the folate receptor (FR) on the targeted cells, leading to increased adenoviral transfection efficiency (Scheme 1d). Ad-Df particles were shown to substantially improve the adenoviral transgene expression in CAR-negative cells. Improvement was observed in transfecting both epithelial cell lines and hematopoietic cells at high and low MOI. Compared to the commercial transfecting agent (Lipofectin) that requires 500 MOI to transfect 40% CAR-negative CT26 cells, our encapsulated Ad only needs 10× lower MOI to reach the same transfection efficiency. When treating hematopoietic cells, the present encapsulated Ad formulation can transfect a higher fraction of hematopoietic cells than other encapsulation techniques at MOI = 200, resulting in a comparative decrease of the transfection failure fraction from 33 to 13%.[35] Two studies were performed in more realistic systems. (1) The encapsulated nonreplicating Ad was shown to efficiently transfect freshly isolated primary patient breast cancer cells in vitro which recapitulates the kind of cellular heterogeneity that is likely to be encountered during intratumoral injection and that may impede the effective delivery. (2) CT26 tumor-bearing mice treated with encapsulated Ad showed an increase of lymphocytes, an improved survival rate, and complete tumor remission. The surviving mice also displayed successful immunity in a rechallenge study which is the first example of therapeutic immune memory with a replicating Ad vector in a DOTAP liposome. These results suggest that the encapsulation method can enhance in vivo Ad transfection and result in a better treatment outcome and has potential to treat aggressive cancers since the more aggressive cancer often expresses a higher level of FRs.[36]

2. MATERIALS AND METHODS

2.1. Reagents and Cell Lines. Replication-deficient Ad-expressing GFP (GFPAd) was purchased from the Baylor College of Medicine (Vector: Ad5-CMV-eGFP). The CT26 cell line was purchased from American Type Culture Collection (ATCC). Replication-competent Ad (TAV255), HEK293, A549, MCF7, and THP-1 cell lines were generously provided from the laboratory of Dr. Tony Reid. Dulbecco's modified Eagle's medium (DMEM) with high glucose (HyClone #SH30081.01) was supplemented with 10% of fetal bovine serum (FBS, Corning #35-011-CV) and 1% of Pen Strep Glutamine (PSG, Life Technologies #10378-016) to prepare the complete media for HEK293, A549, and MCF7 cell culturing. Rosewell Park Memorial Institute (RPMI) 1640 (Gibco #11875093) and RPMI 1640 medium without folic acid (Gibco #27016021) were supplemented with 10% FBS and 1% PSG to prepare the complete RPMI (RP-10) for CT26 and THP-1 cell culturing. Primary human breast cell medium was prepared by supplementing DMEM/F12 (1:1) with HEPES (HyClone #SH30023.01) with 10 mM HEPES (Sigma #H3537), 5% FBS, 1 mg mL^{-1} bovine serum albumin (BSA, Sigma #A7906), 1 $\mu g\ mL^{-1}$ insulin (Invitrogen #51500-056), 0.5 $\mu g\ mL^{-1}$ hydrocortisone (Sigma #H0888), 50 $\mu g\ mL^{-1}$ gentamycin (HyClone #3V30080.01), and 2.5 $\mu g\ mL^{-1}$ Fungizone. Human tumor digestion buffer was prepared with DMEM/F12 + GlutaMAX (Gibco #10565018) supplemented with 10 mM HEPES, 2% BSA, 5 $\mu g\ mL^{-1}$ insulin, 0.5 $\mu g\ mL^{-1}$ hydrocortisone, and 50 $\mu g\ mL^{-1}$ gentamycin. Anti-CAR antibody (clone RmcB, #05-644) was purchased from Millipore, and Alexa Fluor 547-conjugated antibody (polyclonal, #A-21235) was purchased from Invitrogen.

2.2. Liposome-Encapsulated Ad Synthesis. Liposome-encapsulated Ad synthesis was described previously.[53] In brief, DOTAP (Avanti #890890C), cholesterol (Sigma #C3045), 1,2-distearoyl-*sn*-glycero-3-phosphoethanolamine-*N*-[carboxy(polyethylene glycol)-2000] [PEG(2000)-PE carboxylic acid, Avanti #880135P], and 1,2-distearoyl-*sn*-glycero-3-phosphoethanolamine-*N*-[folate(polyethylene glycol)-2000] [PEG(2000)-folate-PE, Avanti #880124P] were suspended in chloroform at a molar ratio of 1:0.26:0.02:0.01. The lipid mixture was vortexed in an amber vial for 30 min at 25 °C. The mixture was vacuumed overnight to form a dry lipid film. The next day, 5×10^{10} vp mL^{-1} of Ad solution was prepared in PBS. The dried lipid film was hydrated with 400 μL of Ad solution while vortexing. The hydrated film was stirred at 600 rpm at 4 °C for 30 min. The sample was transferred to a 2 mL U-bottomed Eppendorf tube and sonicated in an ultrasonic water bath (Fisher Scientific, model FS11011) for 10 min at 4 °C. The suspension was stabilized at 4 °C for 3 h, resulting in DOTAP-folate Ad liposomes (Ad-Df). Replication-deficient Ad (GFPAd) and replication-competent Ad (TAV255) were used for Ad-Df synthesis and denoted as GFPAd-Df and TAV255-DF, respectively. 1/1×, 1/3×, 1/5×, 1/7×, and 1/10× Ad-Df represent the Ad to DOTAP lipid ratio (vp/nmol) 5.17×10^6, 1.55×10^7, 2.59×10^7, 3.62×10^7, and 5.17×10^7, respectively. Ad-Df was characterized by dynamic light scattering (DLS) and cryo-transmission electron microscopy (Cryo-EM). The mean hydrodynamic particle size, polydispersity index (PDI), and zeta potentials were measured using a Malvern Zetasizer Nano-ZS (Malvern Panalytical, Malvern, UK). For Cryo-EM sample preparation, 3 μL of the sample solution was applied to the carbon R2/2 copper grid (Quantifoil Micro Tools GmbH, Jena, Germany). A Leica EMGP plunger (Leica Microsystems Inc., Illinois, USA) was used for blotting at room temperature and 95% humidity. The frozen and hydrated grid was loaded on a precooled Gatan cryo-transfer holder (Gatan, Inc., California, USA) and imaged by JEOL JEM-2100F (JEOL USA, Massachusetts, USA) at 200 kV. Fiji software was used for image processing.

2.3. Transfection. Cells were plated overnight at 3×10^4 cells $well^{-1}$ in a 96-well plate at 37 °C and 5% CO_2 in the complete media. GFPAd, 1/1×, 1/3×, 1/5×, 1/7×, and 1/10× GFPAd-Df were added to cells (day 1) at a MOI ranging from 3.1 to 400 and incubated at 37 °C and 5% CO_2. GFP fluorescence was measured on days 2, 3, 4, 5, and 6 for HEK293, A549, MCF7, THP-1, and CT26, respectively. GFP-positive cells were counted microscopically using a Keyence BZ-X710 microscope with a GFP filter and 470/40 nm excitation wavelength, 525/50 nm emission wavelength, and dichroic mirror wavelength 495 nm. GFP fluorescence intensities were measured using a Tecan Infinite M200 microplate reader.

2.4. Human Breast Cell Isolation and Culturing. All human breast cancer biospecimens were obtained from patients through Biorepository and Tissue Technology Shared Resources (BTTSR) at UCSD. Patient consent was obtained by BTTSR, and all procedures were conducted under an Institutional Review Board-approved protocol (#181755). Tumor fragments were acquired from two different areas of the same tumor when possible. During the transportation, the acquired tumor tissues were placed in a 50 mL

https://doi.org/10.1021/acsbiomaterials.2c00966
ACS Biomater. Sci. Eng. 2022, 8, 5199−5209

conical tube with sterile PBS such that the tissue sample was entirely submerged in PBS. 2 mg mL^{-1} of type 3 collagenase (Worthing #LS004182) and hyaluronidase (Sigma #H3884) 100 U mL^{-1} in human tumor digest buffer were prepared. Per gram of the tissue, 10 mL of digestion buffer containing enzymes was added into a well in a 6-well plate. Tissue was placed into the well and minced until finely chopped. If needed, a syringe plunger was used to smash the tumor. The resultant tissue was incubated at 37 °C and 5% CO_2 with pipette mixing performed every 30 min. After 5 h of incubation, tissue was strained using a 100 μm strainer, and the filtrate was centrifuged at 530*g* at room temperature for 5 min to collect cells. If red blood cells were observed, then 5−10 mL of ACK buffer (Quality Biological #118-156-101) was added and incubated for 3 min. Cells were centrifuged at 530*g* at 25 °C for 5 min, and the supernatant was removed. This step was repeated until the red blood cells were no longer visible. The resultant cells were resuspended in 10 mL of the primary human breast cell medium, and an aliquot of 10 μL was used for cell counting. Cells were plated at minimal 10,000 cells $well^{-1}$ in a 96-well plate. Viral infection was performed after cells attached to the well (24−48 h after plating).

2.5. Hexon Staining. Cells were plated in a 96-well plate at approximately 3×10^4 cells $well^{-1}$ in 100 μL media/well. The next day, cells were transfected with TAV255, 1/1× TAV255-Df, 1/3× TAV255-Df, 1/5× TAV255-Df, 1/7× TAV255-Df, and 1/10× TAV255-Df (day 1) at a MOI ranging from 3.1 to 400 at 37 °C and 5% CO_2. At the end of transfection, the medium was gently pipetted off, and 50 μL $well^{-1}$ of cold methanol was added and incubated at −20 °C for 20 min. Wells were washed once with 100 μL $well^{-1}$ of PBS-T (Teknova #P3189, diluted to 1× in PBS). 100 μL $well^{-1}$ of StartingBlock (Thermo #37542) was added to block the cells for 30 min at room temperature. 50 μL $well^{-1}$ of diluted anti-hexon (Thermo #MA1-7326, diluted 1:500 in StartingBlock) was added and incubated for 1 h at room temperature. After washes with 100 μL $well^{-1}$ of PBS-T, 50 μL $well^{-1}$ of HRP anti-mouse (Cell Signaling #7076, diluted 1:500 in StartingBlock) was added and incubated for 30 min at room temperature. DAB was prepared by mixing 3 μL of the concentrate per 100 μL diluent from the kit (Cell Signaling #8059P). The plate was washed with 100 μL $well^{-1}$ of PBS-T twice, and 40 μL $well^{-1}$ of the DAB substrate was added into the wells. After the cells were sufficiently stained, as observed under a microscope, DAB was discarded, and 100 μL $well^{-1}$ of PBS was added. Hexon-positive cells were imaged and counted under a microscope.

2.6. Cell Viability Assay. Cells were seeded in a 96-well plate at approximately 3×10^4 cells $well^{-1}$ in 100 μL media $well^{-1}$. The next day, TAV255, 1/3× TAV255-Df, and 1/10× TAV255-Df were added to cells (day 1) at a MOI ranging from 3.1 to 400 and incubated at 37 °C and 5% CO_2. On days 2, 4, and 6 post-infection, 1×10^4 cells were harvested and incubated with Alamar Blue for 1−4 h. The cell viability was determined by measuring absorbance at wavelengths of 570 and 600 nm.

2.7. Animals. Six to eight week old female BALB/cAnNHsd mice were purchased from Envigo RMS, LLC. 5×10^5 of CT26 cells in 50 μL of PBS were subcutaneously injected. Tumor volume was determined by a caliper with the modified ellipsoidal formula: volume (mm^3) = (width × width × length)/2, and treatment was started at a tumor size of approximately 23 mm^3. 5×10^9 vp of TAV255 or 1/10× TAV255-Df, or equivalent 1/10× Df, or PBS was intratumorally injected every other day. Pain and distress in tumor-bearing mice were closely monitored. For the survival study, mice were euthanized when a tumor ulcerated or reached 1500 mm^3. All procedures and protocols were approved by the UC San Diego Institutional Animal Care and Use Committee (IACUC).

2.8. CAR Analysis. Cells were incubated with anti-CAR antibody at 1:500 dilution in BD staining buffer at 4 °C for 30 min. Cells were washed once with BD staining buffer and incubated with secondary Alexa Fluor 647-conjugated antibody at 1:400 dilution in BD staining buffer for 30 min at 4 °C. The stained cells were washed twice with BD staining buffer and resuspended in 200 μL of PBS. The stained cells were analyzed by BD FACSCalibur flow cytometry.

2.9. TIL Analysis. CT26-bearing mice were first treated at a tumor size of approximately 70 mm^3. A 2.5×10^9 vp of TAV255 or 1/10× TAV255-Df in 50 μL of PBS was injected i.t. on days 0, 2, 4, 6, 8, and 10. Mice were sacrificed on day 12 for TIL analysis. Tumors were dissociated into cell suspensions using collagenase D (Roche #11088866001) at 1 mg mL^{-1} in RP10. Cell suspensions were incubated with cocktails of anti-mouse CD45 (BioLengend #103114), anti-mouse CD3 (BD Biosciences #553062), and anti-mouse CD8 (eBiosciences #48-0081) antibodies at 4 °C for 30 min. Fixation and Permeabilization Solution kits were used for IFN-γ staining (eBiosciences #17-7311). The stained cells were analyzed by BD FACSCanto flow cytometry.

2.10. Stability in Serum. Neutralizing serum was prepared by administering, intravenously, three doses (5×10^9 VP/dose) of Ad-GFP (Vector Development Lab, Baylor College of Medicine) to Balb/c mice (The Jackson Laboratory) over 10 days. Blood was collected from the mice via cardiac puncture. Blood was left to coagulate at room temperature for 30 min before being centrifuged at 15,000*g* for 10 min. The supernatant was collected as the designated neutralizing serum. The serum was then decomplemented by heating it in a water bath at 56 °C for 30 min and stored at −80 °C until use.

3. RESULTS AND DISCUSSION

3.1. Encapsulated Virus Transfected CAR^+ and CAR^- Cells. The synthesis of coated Ad is illustrated in Scheme 1a. A lipid film composed of DOTAP, cholesterol, 1,2-distearoyl-*sn*-glycero-3-phosphoethanolamine-*N*-[carboxy(polyethylene glycol)-2000] [PEG(2000)-PE carboxylic acid], and 1,2-distearoyl-*sn*-glycero-3-phosphoethanolamine-*N*-[folate(polyethylene glycol)-2000] [PEG(2000)-folate-PE] was used to encapsulate Ad, producing Ad-DOTAP-folate liposomes (Ad-Df). 1/1×, 1/3×, 1/5×, 1/7×, and 1/10× Ad-Df represent the Ad viral particle (vp) to DOTAP lipid (nmol) ratios of 5.17×10^6, 1.55×10^7, 2.59×10^7, 3.62×10^7, and 5.17×10^7, respectively. Two types of Ad were used to evaluate the liposome encapsulation procedure: A recombinant human Ad expressing GFP (GFPAd, non-replicable) and a tumor-selective oncolytic Ad (TAV255, replicable in tumor cells). Ad, empty liposome, and encapsulated Ad (Ad-Df) were characterized by DLS and are summarized in Table 2. The measurements showed the increase in size from

Table 2. Physiochemical Characterization of Df, DfA, and Naked Ad

formulation	*z*-average (nm)	PDI	ζ potential (mV)
empty Df	689 ± 67	0.31 ± 0.18	6.1 ± 0.1
naked GFPAd	126 ± 2	0.17 ± 0.02	−2.9 ± 1.8
naked TAV255	120 ± 2	0.12 ± 0.02	−7.1 ± 1.3
Ad-Df (GFPAd)	812 ± 124	0.51 ± 0.17	2.5 ± 0.3
Ad-Df (TAV255)	759 ± 51	0.60 ± 0.05	3.7 ± 0.7

126 ± 2 nm (before encapsulation) to 812 ± 124 nm (after encapsulation) for GFPAd or from 120 ± 2 nm (before encapsulation) to 759 ± 51 nm (after encapsulation) for TAV255. The PDI was 0.17 ± 0.02 for naked GFPAd and 0.12 ± 0.02 for naked TAV255. After encapsulation, the PDI increased to 0.51 ± 0.17 (encapsulated GFPAd) and 0.60 ± 0.05 (encapsulated TAV255), respectively. Naked Ad and encapsulated Ad (Ad-Df) were examined under Cryo-EM to evaluate their encapsulation efficiency. Based on 30 Cryo-EM images, all Ad appears to be encapsulated inside liposomes, indicating that the encapsulation rate is approximately 100% (Figure 1).

A recombinant human Ad-expressing GFP (GFPAd) was used to determine the transfection efficiency by quantifying the percentage of GFP-positive cells after infection. HEK293 (human embryonic kidney cells), A549 (human lung cancer cells), MCF7 (human breast cancer cells), CT26 (mouse colon cancer cells), and THP-1 (human monocytes) cell lines were

https://doi.org/10.1021/acsbiomaterials.2c00966
ACS Biomater. Sci. Eng. 2022, 8, 5199−5209

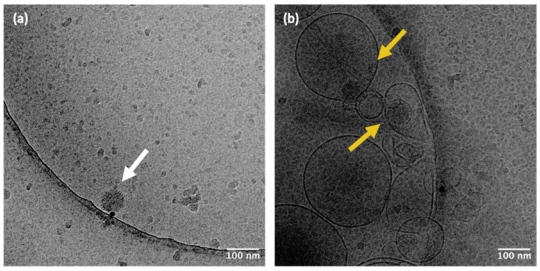

Figure 1. Cryo-EM image reveals the successful encapsulation of Ad. (a) Naked Ad. White arrow indicates the naked Ad. (b) Df-Ad. Yellow arrows indicate the Ad-encapsulated liposomes. The images were taken under 15,000× magnification. The scale bars in the image indicate 100 nm.

chosen to assess the transfection efficiency of naked GFPAd and encapsulated GFPAd in DOTAP-folate liposome (GFPAd-Df) in cell lines with various expression levels of CAR. The levels of CAR expression were reported previously[41−44] and were also examined by flow cytometry (Supporting Information, Figure S1). HEK293 and A549 are CAR-positive cell lines and MCF7, CT26, and THP-1 are CAR-negative cell lines. From MOI = 1.6 to 100, GFPAd and GFPAd-Df transfect CAR-positive cells, and there is no significant difference between naked GFPAd and GFPAd-Df or among the different Ad-to-lipid ratio variants of GFPAd-Df (Figure 2a,b). 1/1× GFPAd-Df on HEK293 cells demonstrated a reduced percentage of GFP-positive cells at MOI = 100 which is likely because high concentrations of DOTAP are cytotoxic to cells.[45] The cytotoxicity of the liposomes was performed on a 96-well plate by incubating empty sonicated DOTAP liposomes with 3×10^4 cells in 200 μL of cell media for 5 days at 37 °C with CO^2 to determine the half-maximal inhibitory concentration (IC_{50}). High-concentration DMSO-treated cells were used as a positive control and untreated cells were used as a negative control for calculating the percentage of live cells. The IC_{50} of the DOTAP liposomes on CT26 is 75.7 μM which is much higher than the concentration of liposomes we used for the transfection studies (Supporting Information, Figure S2). 1/3× to 1/10× GFPAd-Df showed a proportional increase in GFP-positive cells when increasing MOI. Ad-Df remained stable for at least 30 days and could transfect cells with ∼80% of transfection efficiency compared to the freshly made Ad-Df (Supporting Information, Figure S3). The stability of Ad-Df in the presence of blood proteins was documented by the experiment of the transfection efficiency of Ad-Df after exposing to serum showing that the Ad-Df is stable in the serum for at least 1 h which is equal to a large number of circulation cycles in the human vasculature (Supporting Information, Figure S4).

In MCF7 and CT26 cell lines, GFPAd infection of cells with low levels of CAR resulted in low levels of GFP expression, as expected (Figure 2c,d). In contrast, GFPAd-Df infected CAR-negative cells and synthesized high levels of GFP, which suggest that GFPAd encapsulated in liposomes can transfect cells by a CAR-independent manner. The percentage of GFP-positive cells was 4- to 32-fold higher in GFPAd-Df-transfected MCF7 than in GFPAd-transfected MCF7 (Figure 2c). Uncoated Ad only showed subtle GFP expression at high MOI (MOI > 100) and was unable to detectably transfect CAR-negative cells at MOIs below MOI 25. Conversely, GFPAd-Df was able to transfect CAR-negative cells at all MOIs (as low as 3.1 MOI, Supporting Information, Figures S5 and S6). Folate in the liposome formulation improved the transfection efficiency in CAR^-FR^+ CT26 cells (Supporting Information, Figure S5) which is likely due to a cellular internalization improvement from the folate-mediated endocytosis.[46]

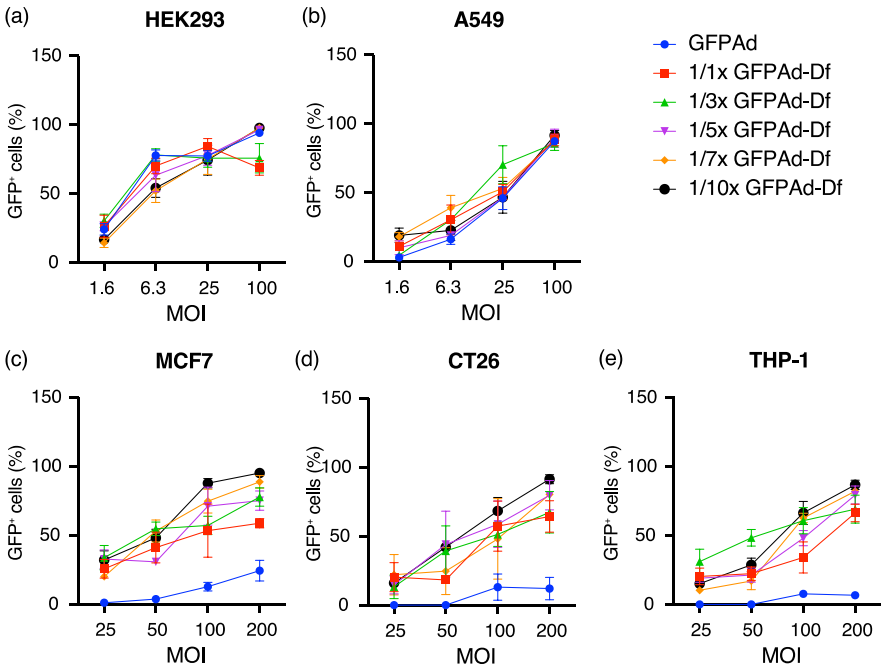

Figure 2. Liposomal encapsulation enhances the transfection efficiency in CAR-negative and CAR-positive cells. (a) HEK293 and (b) A549 were transfected with GFPAd, 1/1× GFPAd-Df, 1/3× GFPAd-Df, 1/5× GFPAd-Df, 1/7× GFPAd-Df, and 1/10× GFPAd-Df at MOI = 1.6, 6.3, 25, and 100. CAR-negative cells (c) MCF7, (d) CT26, and (e) THP-1 were transfected with GFPAd, 1/1× GFPAd-Df, 1/3× GFPAd-Df, 1/5× GFPAd-Df, 1/7× GFPAd-Df, and 1/10× GFPAd-Df at MOI = 25, 50, 100, and 200 for CAR^- cells. GFP^+ cells were counted under a Keyence BZ-X710 fluorescence microscope on days 2, 3, 4, 5, and 6 for HEK293, A549, MCF7, THP-1, and CT26, respectively.

https://doi.org/10.1021/acsbiomaterials.2c00966
ACS Biomater. Sci. Eng. 2022, 8, 5199−5209

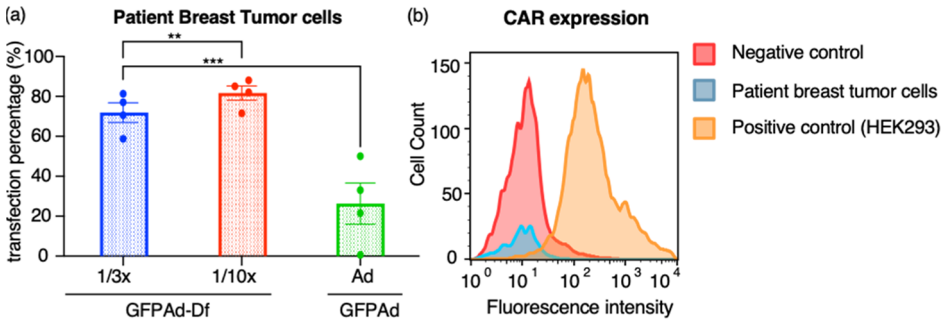

Figure 3. Encapsulated virus efficiently transfects patients' breast tumor cells. (a) Transfection percentage in primary patient breast tumor cells. Patients' breast tumors were obtained from four different surgeries ($n = 4$) and dissociated in protease and hyaluronidase enzyme solution for 5−8 h at 37 °C. Harvested cells were transfected with GFPAd, 1/3× GFPAd-Df, and 1/10× GFPAd-Df at MOI = 100. Transfection percentage was shown as the GFP-positive cell percentage. GFP-positive cells were counted under a Keyence BZ-X710 fluorescence microscope on day 4 after infection. (b) Patients' breast tumor cells are predominantly CAR-negative cells. One CAR analysis result is shown as the representative of four independent experiments of similar results. ** means $p < 0.01$ and ***means $p < 0.001$.

Since GFPAd-Df was shown to transfect CAR-deficient epithelial cancer cells (Figure 2c), the transfection capability in other cell types was also investigated. In contrast to adherent cells, suspension cells and particularly hematopoietic cells are notoriously difficult to transfect.[47] In the study presented in Figure 2e, THP-1, a human monocytic leukemia cancer, and CAR-deficient cell line[48] were used to estimate the transfection capability of GFPAd-Df in the suspensions of hematopoietic cells. THP-1 cells were transfected with naked GFPAd and GFPAd-Df at MOI 25−200. A negatively charged folate-lecithin liposome-coated GFPAd (1/10× GFPAd-Lf) was used as a control to compare the transfection efficiency of encapsulated GFPAd (Supporting Information, Figure S6). The transfection efficiency of negatively charged liposome-encapsulated GFPAd was improved compared to the naked GFPAd in THP-1 cells (CAR-negative). The transfection performed with cationic 1/10× GFPAd-Df showed the strongest GFP expression among all groups and raised the number of GFP-positive cells more than 10× compared to naked GFPAd. Encapsulated GFPAd strongly enhances GFPAd entry into CAR-deficient cancer cells and allows transfer of viral genes with MOIs below 25. The positive charge of the liposomes most likely interacts with the negatively charged cell surface to increase the probability of cell internalization. These results show that GFPAd poorly transfects the cells without CAR expressed on the cell surface, and liposome encapsulation can eliminate the strong dependency on CAR expression for cellular entry. Additionally, GFPAd-Df can effectively transfect various types of cells, which include epithelial cancer cells and suspended hematopoietic cells.

3.2. Encapsulated Virus Efficiently Transfects Patients' Breast Tumor-Derived Cells. To model the diverse landscape of human cancers, patient-derived tumor cells were employed as a preclinical model to study the transfection efficiency of the non-encapsulated and encapsulated Ad. Replication-defective GFPAd was used to determine the transfection efficiency by quantifying the percentage of GFP-positive cells after infection. Breast tumor tissues were surgically removed from four patients and dissociated at the laboratory to form single cell suspensions. Patient-derived breast cancer single cells were plated and incubated at 37 °C in 5% CO_2 for 1−2 days. After the cells adhered to the plate, they were transfected with GFPAd, 1/3× GFPAd-Df, or 1/10× GFPAd-Df at MOI = 100, and the transfection efficiency in primary human tumor cells was quantified by counting the percentage of GFP-positive cells. A relatively high lipid to Ad ratio formula (1/3× GFPAd-Df) and low lipid to Ad ratio formula (1/10× GFPAd-Df) were used to confirm that the transfection performance in primary cells is similar to that in the cell lines. 1/1× GFPAd-Df was not chosen due to potential cytotoxicity from high concentrations of lipid at high MOI. In Figure 3a, 1/3× GFPAd-Df, 1/10× GFPAd-Df, and GFPAd showed 72, 82, and 26% of GFP-positive cells in patients' primary breast tumor cells, respectively. Flow cytometry analysis (Figure 3b) indicates that most cells derived from the patients are CAR-deficient. These data show that GFPAd-Df is capable of transfecting primary human tumor cells with negative CAR expression on the cell surface, so Ad encapsulated in DOTAP-folate liposome is a promising candidate for clinical translation because it promotes effective and broad transfection.

3.3. Replicating Virus Encapsulated in Liposomes in CAR-Negative Cells. After showing that the encapsulated Ad can transfect CAR-deficient cells using replication-deficient GFPAd (Figures 2 and 3), a replicating Ad was used with the same liposome formulas to ensure that the replicating virus is able to undergo liposomal delivery in a similar way. TAV255, a tumor-selective replicating oncolytic Ad,[49] was encapsulated in DOTAP-folate liposomes to evaluate the transfection efficiency in CAR-deficient cells. TAV255 has a 50 nucleotide deletion in the promoter of E1A, and it showed potent tumor-selective oncolytic activity in CAR-positive cells in vitro and in vivo. A previous study demonstrated that TAV255 could effectively replicate in tumor cells but had a remarked reduction of replication in normal cells.[49] Hexon, the most abundant structural protein in the Ad capsid,[50] was used to quantify the transfection efficiency. CAR-negative CT26 cells were transfected with TAV255, 1/3× TAV255-Df, and 1/10× TAV255-Df at MOI = 400, and hexon was stained for visualization (Figure 4a−c). 1/3× TAV255-Df and 1/10× TAV255-Df displayed an increased amount of the hexon protein compared to TAV255. The hexon expression was analyzed and quantified using ImageJ Fiji software[51] and is shown in Figure 4d. 1/3× TAV255-Df and 1/10× TAV255-Df had a 26- and 28-fold increase in hexon expression in CT26 cells compared to non-encapsulated TAV255. These results indicated that the replicating virus encapsulated in liposomes showed improved adenoviral transfection efficiency. Since hexon is encoded by viral late genes,[52] the hexon expression in TAV255-Df-infected cells suggests that TAV255-Df was able to reach the late stage of viral gene transcription. The enhanced transfection efficiency of the replicating virus in liposomes also suggests that such a coating

https://doi.org/10.1021/acsbiomaterials.2c00966
ACS Biomater. Sci. Eng. 2022, 8, 5199−5209

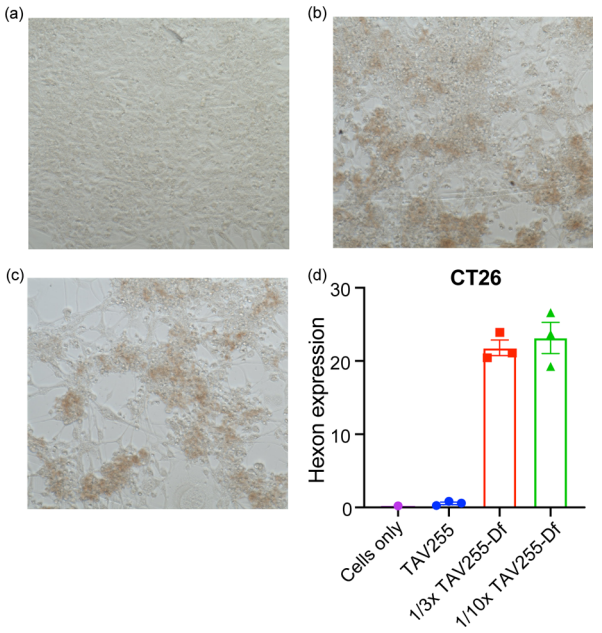

Figure 4. Replicating virus encapsulated in liposomes in CAR-negative CT26 cells. (a–d) CT26 was transfected with TAV255, 1/3× TAV255-Df, and 1/10× TAV255-Df using a replicating TAV255 virus. Representative image of hexon staining in (a) TAV255, (b) 1/3× TAV255-Df, and (c) 1/10× TAV255-Df infected CT26. (d) Hexon expression of non-encapsulated and encapsulated TAV255 in CT26. Data are shown as mean with standard errors of the mean.

formulation can be used for cancer treatments that deliver oncolytic viruses to tumor cells which express viral genes, replicate inside the tumor cells, and eventually lyse to kill the tumor cells.

3.4. Cell Viability of Replicating Virus Encapsulated in Liposomes in CAR$^+$ and CAR$^-$ Cells. To verify that the encapsulated replicating Ad (TAV255) can kill targeted tumor cells after transfection, an Alamar Blue assay was used to determine cell viability after transfection. In Figure 5a–c, both TAV255 and encapsulated TAV255 kill CAR-positive tumor cells, such as A549. The killing ability is correlated to the incubation time and MOIs. In CAR-negative tumor cells, CT26 and TAV255 showed a very limited killing ability for tumor cells, and encapsulated TAV255 (1/3× and 1/10× TAV255-Df) demonstrated an enhanced tumor cell killing ability (Figure 5d–f). On day 6 post-infection, 1/10× TAV255-Df had a fivefold and twofold higher killing ability than naked TAV255 at MOI = 400 and MOI = 200, respectively. Encapsulating TAV255 in liposomes overcomes the limited clinical applicability of conventional oncolytic Ad. Taken together, the results from Figures 4 and 5 show that TAV255-Df can effectively transfect and kill CAR-negative tumor cells and can be a powerful alternative to naked, that is, unencapsulated TAV255.

3.5. Encapsulated Ad Suppresses Tumor Growth. Oncolytic adenoviruses, being potent tumor lysing agents, can kill tumor cells and release tumor antigens to stimulate the immune response against tumors. The above data (Figure 4) showed that the liposomes were effective in enhancing viral gene transfection in CAR-negative cells with a replicating Ad. To investigate the immune response, an immune-competent mouse model is desired for in vivo studies. A CAR-negative human

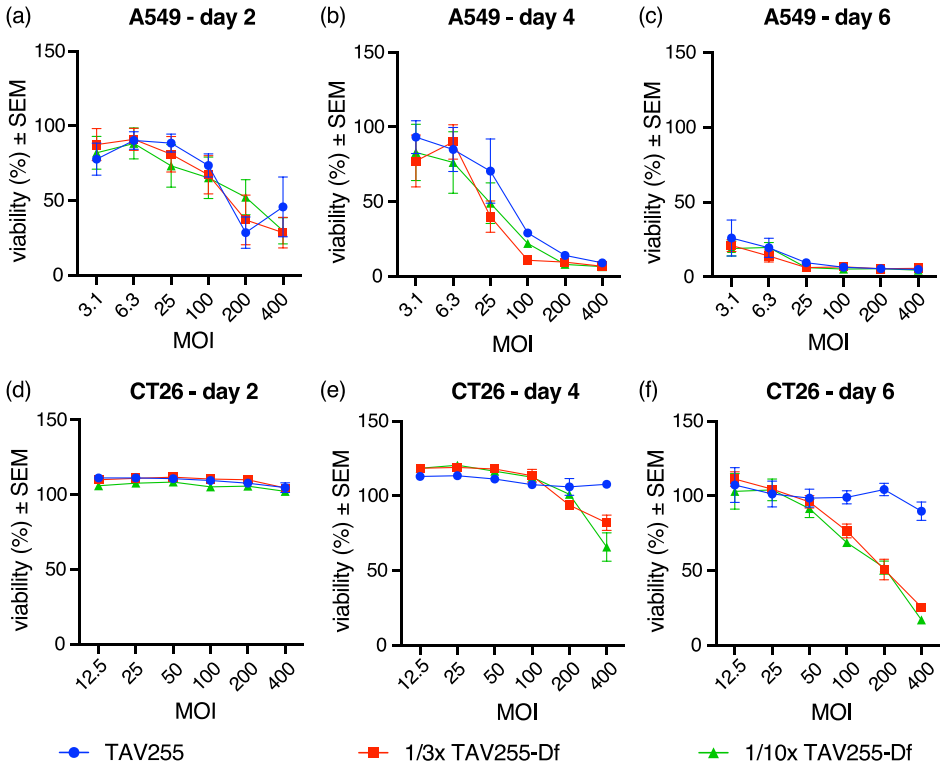

Figure 5. Viability of the replicating virus encapsulated in liposomes in CAR$^+$ and CAR$^-$ cells. (a–c) A549 cells (CAR$^+$) were transfected with TAV255, 1/3× TAV255-Df, and 1/10× TAV255-Df. (d–f) CT26 cells (CAR$^-$) were transfected with TAV255, 1/3× TAV255-Df, and 1/10× TAV255-Df. Cell viability was measured on days 2, 4, and 6 post-infection with the Alamar Blue assay. Data are shown as the mean with standard errors of the mean (SEM).

https://doi.org/10.1021/acsbiomaterials.2c00966
ACS Biomater. Sci. Eng. 2022, 8, 5199–5209

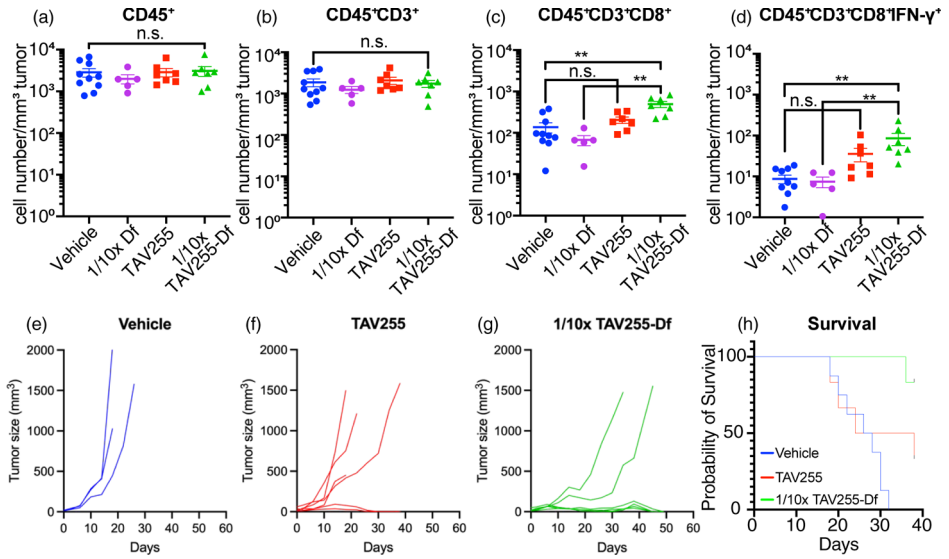

Figure 6. Encapsulated Ad suppresses tumor growth. PBS, 1/10× Df, TAV255, and 1/10× TAV255-Df (n = 5−10) were intratumorally injected every other day. (a−d) Analysis of infiltrating lymphocytes in the tumor microenvironment by flow cytometry. (e−g) Tumor progression curve for PBS (vehicle, n = 3), TAV-255 (n = 6), and 1/10× TAV255-Df (n = 6). The curves were splined fitted by averaging sizes every four days and plotted. (h) Survival curve comparing treatment with PBS (vehicle, n = 8), TAV255 (n = 6), and 1/10× TAV255-Df (n = 6). Data are shown as mean with standard errors of the mean (SEM). * means $p < 0.05$ and ** means $p < 0.01$.

breast cancer model would be ideal, but CAR-negative patient-derived breast tumors cannot be used in immune-competent mice. Consequently, a CT26 (murine cell line) model in an immune-competent mouse model (Balb/c, immune-competent mouse) was studied even though CT26 is a colon cancer cell line because CT26 has lower CAR expression than any convenient (fast growing) murine breast cancer cell line. Given the known efficacy of encapsulated TAV255 in CT26 in vitro, encapsulated TAV255 (TAV255-Df) was used in a mouse study. Four treatment groups were used to elucidate the effect of virus encapsulation: (1) vehicle, (2) empty liposome (1/10× Df), (3) naked Ad (TAV255), and (4) coated Ad (1/10× TAV255-Df). The agents were intratumorally (i.t.) injected every other day for six doses. Tumors were harvested on day 12 after the first treatment to investigate the tumor-infiltrating lymphocytes (TILs) in the tumor environment. In Figure 6a−d, the 1/10× TAV255-Df-treated group showed a higher number of infiltrating killer T cells ($CD45^+CD8^+$) in the tumors compared to the other treatments. About a 10-fold increase in IFN-γ^+-killer T cells ($CD45^+CD8^+IFN\text{-}\gamma^+$) was observed in tumors following the 1/10× TAV255-Df therapy compared to vehicle, indicating the activation of cytotoxic T cells to destroy the tumor cells (Figure 6f).

The increase of immune cells and IFN-γ^+ T cells in tumors indicates an improved immune response brought about by the 1/10× TAV255-Df therapy. The enhanced immune responses (Figure 6a−d) and tumor cell killing ability (Figure 5) also reflect on the tumor growth inhibition. In Figure 6e−g, the 1/10× TAV255-Df-treated group demonstrated the best inhibition of tumor growth. Four out of six CT26 tumors were induced into full remission by the 1/10× TAV255-Df treatment (~67% full remission rate), compared to two out of six tumors that were induced into full remission by TAV-255 (~33% full remission rate). The accumulative dose of 8.5×10^8 PFU of the TAV255-Df in this treatment was lower than the accumulative doses of 5×10^9 PFU of the oncolytic virus which showed no toxicity in animals, suggesting that the current dosages are safe for the treatment. The cured mice were closely monitored, and none of them had tumor recurrence. On day 53, 10^6 CT26 cells were injected to rechallenge the cured mice with no further treatment, and none of them regrew tumors in the 1/10× TAV255-Df-treated group (immunity to the rechallenge rate: 100%), indicating that the encapsulated virus induced a tumor-specific memory response. In addition, the 1/10× TAV255-Df treatment significantly improved the survival rates (Figure 6h). On 38 day post-treatment, 83% of mice were alive in the 1/10× TAV255-Df-treated group, while 33 and 0% of mice were alive in TAV255- and PBS-treated groups, respectively. These results demonstrate that encapsulating Ad in liposomes with folate modification can promote immune cell infiltration, suppress tumor growth, and improve survival. Other oncolytic viruses can also be encapsulated with the same formulation in order to induce a stronger immune response. For instance, oncolytic viruses with immunostimulatory protein-encoding genes can be encapsulated in DOTAP-folate liposomes to stimulate and induce a more robust immune response to fight against cancer.

4. CONCLUSIONS

Liposomal encapsulation is a well-understood strategy to reduce the immune recognition and elimination of adenoviruses in the bloodstream, which are otherwise unsuitable for a systemic delivery, given the prevalence of neutralizing antibodies arising from frequent childhood infections. The in vivo oncologic application of adenoviruses may also be limited by the lack of the requisite CAR in tumor cells. In this study, the transfection efficiency of Ad encapsulated in cationic DOTAP-folate liposomes was investigated in CAR-positive cells and CAR-negative cells. Encapsulation enhanced the adenoviral GFP protein expression in CAR-negative cells. As shown in the patients' breast tumor-derived cells, encapsulated Ad transfected 3× higher in primary human cancer cells than in the non-encapsulated Ad, and these primary cells were found to be CAR-deficient. When encapsulated replicating Ad was intratumorally administrated to treat a murine colorectal cancer model (CT26, CAR-negative), a 3.6× increase in TILs and full tumor remission was observed. Encapsulation of Ad in the liposome formula

https://doi.org/10.1021/acsbiomaterials.2c00966
ACS Biomater. Sci. Eng. 2022, 8, 5199−5209

improved survival rates 2.5× compared to non-encapsulated Ad. To our knowledge, this study is the first to demonstrate that the encapsulation of a replicating oncolytic Ad in DOTAP liposomes, by comparison with unencapsulated Ad, leads to improved regression of tumors, increased survival, long-term remissions, and full protection from tumor rechallenge in 100% of previously cured animals. In summary, DOTAP-folate-encapsulated Ad may provide a method to efficiently transport Ad into cells regardless of the CAR expression. The enhanced transfection efficiency of the liposome-encapsulated Ad makes Ad-Df a promising reagent in cancer gene therapy.

■ ASSOCIATED CONTENT

Supporting Information

The Supporting Information is available free of charge at https://pubs.acs.org/doi/10.1021/acsbiomaterials.2c00966.

CAR expression in various cell lines, cytotoxicity of liposomes, storage stability of Ad-Df, stability of Ad-Df in serum, improvement of folate-targeting in FR+ cells by Ad-DF, and transfection of monocytes by Ad-Df (PDF)

■ AUTHOR INFORMATION

Corresponding Author

Andrew C. Kummel − *Department of Chemistry & Biochemistry, University of California San Diego, La Jolla, California 92093, United States;* orcid.org/0000-0001-8301-9855; Email: akummel@ucsd.edu

Authors

Ching-Hsin Huang − *Moores Cancer Center, University of California San Diego, La Jolla, California 92037, United States;* orcid.org/0000-0002-8396-3878

Tao Dong − *Moores Cancer Center, University of California San Diego, La Jolla, California 92037, United States;* orcid.org/0000-0002-9506-9136

Abraham T. Phung − *Moores Cancer Center, University of California San Diego, La Jolla, California 92037, United States*

Jaimin R. Shah − *Moores Cancer Center, University of California San Diego, La Jolla, California 92037, United States*

Christopher Larson − *EpicentRx, Inc., La Jolla, California 92037, United States*

Ana B. Sanchez − *EpicentRx, Inc., La Jolla, California 92037, United States*

Sarah L. Blair − *Moores Cancer Center, University of California San Diego, La Jolla, California 92037, United States*

Bryan Oronsky − *EpicentRx, Inc., La Jolla, California 92037, United States;* orcid.org/0000-0002-3940-6329

William C. Trogler − *Department of Chemistry & Biochemistry, University of California San Diego, La Jolla, California 92093, United States;* orcid.org/0000-0001-6098-7685

Tony Reid − *EpicentRx, Inc., La Jolla, California 92037, United States*

Complete contact information is available at: https://pubs.acs.org/10.1021/acsbiomaterials.2c00966

Notes

The authors declare the following competing financial interest(s): This study was funded by EpicentRx Inc. Tony Reid is the Chief Executive Officer & Chief Scientific Officer at EpicentRx. Christopher Larson is the vice president of viral therapy, Bryan Oronsky is the Chief Medical Officer, and Ana Sanchez is a senior project scientist at EpicentRx. The terms of this arrangement have been reviewed and approved by the University of California San Diego, in accordance with its conflict of interest policies.

■ ACKNOWLEDGMENTS

This research was funded by EpicentRx, Inc., and by a gift from Kreuger V. Wyeth. We would like to acknowledge the UCSD Cancer Center Microscopy Shared Facility Specialized Support Grant (P30 CA23100). We would also like to acknowledge T.R.'s lab for providing us with HEK293, A549, MCF7, and THP-1 cell lines and replication-competent Ad (TAV255) and the UC Irvine Materials Research Institute (IMRI), which is supported in part by the National Science Foundation through the UC Irvine Materials Research Science and Engineering Center (DMR-2011967) for Cryo-EM.

■ REFERENCES

(1) Harrington, K.; Freeman, D. J.; Kelly, B.; Harper, J.; Soria, J.-C. Optimizing Oncolytic Virotherapy in Cancer Treatment. *Nat. Rev. Drug Discovery* **2019**, *18*, 689−706.

(2) Pol, J.; Kroemer, G.; Galluzzi, L. First Oncolytic Virus Approved for Melanoma Immunotherapy. *OncoImmunology* **2016**, *5*, No. e1115641.

(3) Russell, S. J.; Peng, K.-W.; Bell, J. C. Oncolytic virotherapy. *Nat. Biotechnol.* **2012**, *30*, 658−670.

(4) Macedo, N.; Miller, D. M.; Haq, R.; Kaufman, H. L. Clinical Landscape of Oncolytic Virus Research in 2020. *J Immunother Cancer* **2020**, *8*, No. e001486.

(5) Ries, S. J.; Brandts, C. H.; Chung, A. S.; Biederer, C. H.; Hann, B. C.; Lipner, E. M.; McCormick, F.; Michael Korn, W. Loss of P14ARF in Tumor Cells Facilitates Replication of the Adenovirus Mutant Dl1520 (ONYX-015). *Nat. Med.* **2000**, *6*, 1128−1133.

(6) Kirn, D.; Martuza, R. L.; Zwiebel, J. Replication-Selective Virotherapy for Cancer: Biological Principles, Risk Management and Future Directions. *Nat. Med.* **2001**, *7*, 781−787.

(7) Ma, J.; Ramachandran, M.; Jin, C.; Quijano-Rubio, C.; Martikainen, M.; Yu, D.; Essand, M. Characterization of Virus-Mediated Immunogenic Cancer Cell Death and the Consequences for Oncolytic Virus-Based Immunotherapy of Cancer. *Cell Death Discov* **2020**, *11*, 48.

(8) Choi, K.-J.; Kim, J.-H.; Lee, Y.-S.; Kim, J.; Suh, B.-S.; Kim, H.; Cho, S.; Sohn, J.-H.; Kim, G. E.; Yun, C.-O. Concurrent Delivery of GM-CSF and B7-1 Using an Oncolytic Adenovirus Elicits Potent Antitumor Effect. *Gene Ther.* **2006**, *13*, 1010−1020.

(9) D'Alise, A. M.; Leoni, G.; Cotugno, G.; Troise, F.; Langone, F.; Fichera, I.; De Lucia, M.; Avalle, L.; Vitale, R.; Leuzzi, A.; Bignone, V.; Di Matteo, E.; Tucci, F. G.; Poli, V.; Lahm, A.; Catanese, M. T.; Folgori, A.; Colloca, S.; Nicosia, A.; Scarselli, E. Adenoviral Vaccine Targeting Multiple Neoantigens as Strategy to Eradicate Large Tumors Combined with Checkpoint Blockade. *Nat. Commun.* **2019**, *10*, 2688.

(10) Zhang, W.-W. Development and Application of Adenoviral Vectors for Gene Therapy of Cancer. *Cancer Gene Ther* **1999**, *6*, 113.

(11) Sato-Dahlman, M.; Larocca, C. J.; Yanagiba, C.; Yamamoto, M. Adenovirus and Immunotherapy: Advancing Cancer Treatment by Combination. *Cancers* **2020**, *12*, 1295.

(12) Senior, K. ONYX-015 Phase II Clinical Trial Results. *Lancet Oncol* **2001**, *2*, 3.

(13) Zhang, Y.; Bergelson, J. M. Adenovirus Receptors. *J. Virol.* **2005**, *79*, 12125−12131.

(14) Meier, O.; Greber, U. F. Adenovirus Endocytosis. *J. Gene Med.* **2004**, *6*, S152.

(15) Wang, K.; Huang, S.; Kapoor-Munshi, A.; Nemerow, G. Adenovirus Internalization and Infection Require Dynamin. *J. Virol.* **1998**, *72*, 3455−3458.

(16) Nunez, M. I.; Behrens, C.; Woods, D. M.; Lin, H.; Suraokar, M.; Kadara, H.; Hofstetter, W.; Kalhor, N.; Lee, J. J.; Franklin, W.; Stewart, D. J.; Wistuba, I. I. High Expression of Folate Receptor Alpha in Lung Cancer Correlates with Adenocarcinoma Histology and Mutation. *J. Thorac. Oncol.* **2012**, *7*, 833−840.
(17) Yamauchi, Y.; Greber, U. F. Principles of Virus Uncoating: Cues and the Snooker Ball. *Traffic* **2016**, *17*, 569−592.
(18) Wang, Q.; Zhan, Z.; Pan, Y.; Li, J. Expression of Coxsackie and Adenovirurus Receptor and Its Significance in Lung Cancer. *Chin. Clin. Oncol.* **2007**, *4*, 273−276.
(19) Reeh, M.; Bockhorn, M.; Görgens, D.; Vieth, M.; Hoffmann, T.; Simon, R.; Izbicki, J. R.; Sauter, G.; Schumacher, U.; Anders, M. Presence of the Coxsackievirus and Adenovirus Receptor (CAR) in Human Neoplasms: A Multitumour Array Analysis. *Br. J. Cancer* **2013**, *109*, 1848−1858.
(20) Han, S. Y.; Lee, Y. J.; Jung, H. I.; Lee, S. W.; Lim, S. J.; Hong, S. H.; Jeong, J. S. Gene Transfer Using Liposome-Complexed Adenovirus Seems to Overcome Limitations Due to Coxsackievirus and Adenovirus Receptor-Deficiency of Cancer Cells, Both in Vitro and in Vivo. *Exp. Mol. Med.* **2008**, *40*, 427−434.
(21) Kim, S. Y.; Lee, S. J.; Kim, J. K.; Choi, H. G.; Lim, S. J. Optimization and Physicochemical Characterization of a Cationic Lipid-Phosphatidylcholine Mixed Emulsion Formulated as a Highly Efficient Vehicle That Facilitates Adenoviral Gene Transfer. *Int. J. Nanomedicine* **2017**, *12*, 7323−7335.
(22) Lee, E. M.; Hong, S. H.; Lee, Y. J.; Kang, Y. H.; Choi, K. C.; Choi, S. H.; Kim, I. H.; Lim, S. J. Liposome-Complexed Adenoviral Gene Transfer in Cancer Cells Expressing Various Levels of Coxsackievirus and Adenovirus Receptor. *J. Cancer Res. Clin. Oncol.* **2004**, *130*, 169−177.
(23) Hamada, M.; Yura, Y. Efficient Delivery and Replication of Oncolytic Virus for Successful Treatment of Head and Neck Cancer. *Int. J. Mol. Sci.* **2020**, *21*, 7073.
(24) Gregoriadis, G.; Davis, C. Stability of Liposomes Invivo and Invitro Is Promoted by Their Cholesterol Content and the Presence of Blood Cells. *Biochem. Biophys. Res. Commun.* **1979**, *89*, 1287−1293.
(25) Owens, D. E.; Peppas, N. A. Opsonization, Biodistribution, and Pharmacokinetics of Polymeric Nanoparticles. *Int. J. Pharm.* **2006**, *307*, 93−102.
(26) Zhang, Y.; Wu, J.; Zhang, H.; Wei, J.; Wu, J. Extracellular Vesicles-Mimetic Encapsulation Improves Oncolytic Viro-Immunotherapy in Tumors With Low Coxsackie and Adenovirus Receptor. *Front. Bioeng. Biotechnol.* **2020**, *8*, 574007.
(27) Bruckheimer, E.; Harvie, P.; Orthel, J.; Dutzar, B.; Furstoss, K.; Mebel, E.; Anklesaria, P.; Paul, R. In Vivo Efficacy of Folate-Targeted Lipid−Protamine−DNA (LPD-PEG-Folate) Complexes in an Immunocompetent Syngeneic Model for Breast Adenocarcinoma. *Cancer Gene Ther.* **2004**, *11*, 128−134.
(28) Liang, X.; Luo, M.; Wei, X.-W.; Ma, C.-C.; Yang, Y.-H.; Shao, B.; Liu, Y.-T.; Liu, T.; Ren, J.; Liu, L.; He, Z.-Y.; Wei, Y.-Q. A Folate Receptor-Targeted Lipoplex Delivering Interleukin-15 Gene for Colon Cancer Immunotherapy. *Oncotarget* **2016**, *7*, 52207−52217.
(29) Shi, H.; Yang, L.; Wei, W.; Su, X.; Li, X.; Li, M.; Luo, S.; Zhang, H.; Lu, L.; Mao, Y.; Kan, B.; Yang, L. Systemically Administered Liposome-Encapsulated Ad-PEDF Potentiates the Anti-Cancer Effects in Mouse Lung Metastasis Melanoma. *J. Transl. Med.* **2013**, *11*, 86.
(30) Yotnda, P.; Chen, D. H.; Chiu, W.; Piedra, P. A.; Davis, A.; Templeton, N. S.; Brenner, M. K. Bilamellar Cationic Liposomes Protect Adenovectors from Preexisting Humoral Immune Responses. *Mol. Ther.* **2002**, *5*, 233−241.
(31) Wang, L.; Yao, B.; Li, Q.; Mei, K.; Xu, J.-R.; Li, H.-X.; Wang, Y.-S.; Wen, Y.-J.; Wang, X.-D.; Yang, H.-S.; Li, Y.-H.; Luo, F.; Wu, Y.; Liu, Y.-Y.; Yang, L. Gene Therapy with Recombinant Adenovirus Encoding Endostatin Encapsulated in Cationic Liposome in Coxsackievirus and Adenovirus Receptor-Deficient Colon Carcinoma Murine Models. *Hum. Gene Ther.* **2011**, *22*, 1061−1069.
(32) Düzgüneş, N.; Nir, S. Mechanisms and Kinetics of Liposome−Cell Interactions. *Adv. Drug. Delivery Rev.* **1999**, *40*, 3−18.
(33) Qiu, C.; de Young, M. B.; Finn, A.; Dichek, D. A. Cationic Liposomes Enhance Adenovirus Entry via a Pathway Independent of the Fiber Receptor and αv-Integrins. *Hum. Gene Ther.* **1998**, *9*, 507−520.
(34) Wiethoff, C. M.; Nemerow, G. R. Adenovirus Membrane Penetration: Tickling the Tail of a Sleeping Dragon. *Virology* **2015**, *479−480*, 591−599.
(35) Buttgereit, P.; Weineck, S.; Röpke, G.; Märten, A.; Brand, K.; Heinicke, T.; Caselmann, W. H.; Huhn, D.; Schmidt-Wolf, I. G. H. Efficient Gene Transfer into Lymphoma Cells Using Adenoviral Vectors Combined with Lipofection. *Cancer Gene Ther.* **2000**, *7*, 1145−1155.
(36) Meier, R.; Henning, T. D.; Boddington, S.; Tavri, S.; Arora, S.; Piontek, G.; Rudelius, M.; Corot, C.; Daldrup-Link, H. E. Breast Cancers: MR Imaging of Folate-Receptor Expression with the Folate-Specific Nanoparticle P1133. *Radiology* **2010**, *255*, 527−535.
(37) Sudimack, J.; Lee, R. J. Targeted Drug Delivery via the Folate Receptor. *Recent Adv. Cell. Subcell. Mol. Target.* **2000**, *41*, 147−162.
(38) Elnakat, H.; Ratnam, M. Role of Folate Receptor Genes in Reproduction and Related Cancers. *Front. Biosci.* **2006**, *11*, 506−519.
(39) Selby, L. I.; Cortez-Jugo, C. M.; Such, G. K.; Johnston, A. P. R. Nanoescapology: Progress toward Understanding the Endosomal Escape of Polymeric Nanoparticles. *WIREs Nanomedicine Nanobiotechnology* **2017**, *9*, No. e1452.
(40) Zelphati, O.; Szoka, F. C. Mechanism of Oligonucleotide Release from Cationic Liposomes. *Proc. Natl. Acad. Sci. U.S.A.* **1996**, *93*, 11493−11498.
(41) Kanno, T.; Gotoh, A.; Nakano, T.; Tagawa, M.; Nishizaki, T. Beneficial Oncolytic Effect of Fiber-Substituted Conditionally Replicating Adenovirus on Human Lung Cancer. *Anticancer Res.* **2012**, *32*, 4891.
(42) MacLeod, S. H.; Elgadi, M. M.; Bossi, G.; Sankar, U.; Pisio, A.; Agopsowicz, K.; Sharon, D.; Graham, F. L.; Hitt, M. M. HER3 Targeting of Adenovirus by Fiber Modification Increases Infection of Breast Cancer Cells in Vitro, but Not Following Intratumoral Injection in Mice. *Cancer Gene Ther.* **2012**, *19*, 888−898.
(43) Zhang, L.; Hedjran, F.; Larson, C.; Perez, G. L.; Reid, T. A Novel Immunocompetent Murine Model for Replicating Oncolytic Adenoviral Therapy. *Cancer Gene Ther.* **2015**, *22*, 17−22.
(44) Morton, P. E.; Hicks, A.; Ortiz-Zapater, E.; Raghavan, S.; Pike, R.; Noble, A.; Woodfin, A.; Jenkins, G.; Rayner, E.; Santis, G.; Parsons, M. TNFα Promotes CAR-Dependent Migration of Leukocytes across Epithelial Monolayers. *Sci. Rep.* **2016**, *6*, 26321.
(45) Wei, X.; Shao, B.; He, Z.; Ye, T.; Luo, M.; Sang, Y.; Liang, X.; Wang, W.; Luo, S.; Yang, S.; Zhang, S.; Gong, C.; Gou, M.; Deng, H.; Zhao, Y.; Yang, H.; Deng, S.; Zhao, C.; Yang, L.; Qian, Z.; Li, J.; Sun, X.; Han, J.; Jiang, C.; Wu, M.; Zhang, Z. Cationic Nanocarriers Induce Cell Necrosis through Impairment of Na+/K+-ATPase and Cause Subsequent Inflammatory Response. *Cell Res* **2015**, *25*, 237−253.
(46) Choi, P. S.; Lee, J. Y.; Park, J. H.; Kim, S. W. Synthesis and evaluation of 68 Ga-HBED-CC-EDBE-folate for positron-emission tomography imaging of overexpressed folate receptors on CT26 tumor cells. *J. Label. Compd. Radiopharm.* **2018**, *61*, 4−10.
(47) Burke, B.; Sumner, S.; Maitland, N.; Lewis, C. E. Macrophages in Gene Therapy: Cellular Delivery Vehicles and in Vivo Targets. *J. Leukoc. Biol.* **2002**, *72*, 417−428.
(48) Ebbinghaus, C.; Al-Jaibaji, A.; Operschall, E.; Schöffel, A.; Peter, I.; Greber, U. F.; Hemmi, S. Functional and Selective Targeting of Adenovirus to High-Affinity Fcγ Receptor I-Positive Cells by Using a Bispecific Hybrid Adapter. *J. Virol.* **2001**, *75*, 480−489.
(49) Hedjran, F.; Shantanu, K.; Tony, R. Deletion analysis of Ad5 E1a transcriptional control region: impact on tumor-selective expression of E1a and E1b. *Cancer Gene Ther.* **2011**, *18*, 717−723.
(50) San Martín, C.; Burnett, R. M. Structural Studies on Adenoviruses. *Curr. Top. Microbiol. Immunol.* **2003**, *272*, 57−94.
(51) Crowe, A.; Yue, W. Semi-Quantitative Determination of Protein Expression Using Immunohistochemistry Staining and Analysis: An Integrated Protocol. *BIO-Protoc.* **2019**, *9*, No. e3465.

https://doi.org/10.1021/acsbiomaterials.2c00966
ACS Biomater. Sci. Eng. 2022, 8, 5199−5209

(52) Farley, D. C.; Brown, J. L.; Leppard, K. N. Activation of the Early-Late Switch in Adenovirus Type 5 Major Late Transcription Unit Expression by L4 Gene Products. *J. Virol.* **2004**, *78*, 1782−1791.
(53) Mendez, N.; Herrera, V.; Zhang, L.; Hedjran, F.; Feuer, R.; Blair, S. L.; Trogler, W. C.; Reid, T. R.; Kummel, A. C. Encapsulation of Adenovirus Serotype 5 in Anionic Lecithin Liposomes Using a Bead-Based Immunoprecipitation Technique Enhances Transfection Efficiency. *Biomaterials* **2014**, *35*, 9554−9561.

https://doi.org/10.1021/acsbiomaterials.2c00966
ACS Biomater. Sci. Eng. 2022, 8, 5199−5209